日本原子力研究開発機構機関リポジトリ

Japan Atomic Energy Agency Institutional Repository

Title	Atmospheric discharge and dispersion of radionuclides during the Fukushima Dai-ichi Nuclear Power Plant accident, 1; Source term estimation and local-scale atmospheric dispersion in early phase of the accident
Author(s)	Genki Katata, Masakazu Ota, Hiroaki Terada, Masamichi Chino, Haruyasu Nagai
Citation	Journal of Environmental Radioactivity, 109 ; p.103-113
Text Version	Author
URL	http://jolissrch-inter.tokai-sc.jaea.go.jp/search/servlet/search?5033139
DOI	http://dx.doi.org/10.1016/j.jenvrad.2012.02.006
Right	This is the author's version of a work that was accepted for publication in < Journal of Environmental Radioactivity>. Changes resulting from the publishing process, such as peer review, editing, corrections, structural formatting, and other quality control mechanisms, may not be reflected in this document. Changes may have been made to this work since it was submitted for publication. A definitive version was subsequently published in Journal of Environmental Radioactivity,, vol.109, p.103-113(Jul. 2012), http://dx.doi.org/10.1016/j.jenvrad.2012.02.006.

1 **Atmospheric discharge and dispersion of radionuclides during the Fukushima**

2 **Daiichi Nuclear Power Plant accident. Part I: Source term estimation and**

3 **local-scale atmospheric dispersion in early phase of the accident**

4

7

8 **Abstract:**

9   The atmospheric release of ^{131}I and ^{137}Cs in the early phase of the Fukushima

10 Daiichi Nuclear Power Plant (FNPP1) accident from March 12–14, 2011 was estimated

11 by combining environmental data with atmospheric dispersion simulations under the

12 assumption of a unit release rate (1Bq h^{-1}). For the simulation, WSPEEDI-II

13 computer-based nuclear emergency response system was used. Major releases of ^{131}I (>

14 10^{15} Bq h^{-1}) were estimated when air dose rates increased in FNPP1 during the

15 afternoon on March 12 after the hydrogen explosion of Unit 1 and late at night on

16 March 14. The high-concentration plumes discharged during these periods flowed to the

17 northwest and south-southwest directions of FNPP1, respectively. These plumes caused

18   a large amount of dry deposition on the ground surface along their routes. Overall, the

19   spatial pattern of ^{137}Cs and the increases in the air dose rates observed at the monitoring

20   posts around FNPP1 were reproduced by WSPEEDI-II using estimated release rates.

21   The simulation indicated that air dose rates significantly increased in the

22   south-southwest region of FNPP1 by dry deposition of the high-concentration plume

23   discharged from the night of March 14 to the morning of March 15.

24

1. Introduction

From March 12, 2011, a significant amount of radioactive material was accidentally discharged into the atmosphere from the Fukushima Daiichi Nuclear Power Plant (hereafter referred to as FNPP1) which produced areas of high radiation doses over a wide region of Japan (MEXT, 2011a, b). To assess the magnitude of the accident and radiological doses, estimation of the source term of the radionuclides discharged into the atmosphere is required. Soon after the accident the source term of ^{131}I and ^{137}Cs from March 12 to April 5, 2011 was estimated by authors (Chino et al., 2011), using a reverse estimation method. This method calculates the release rates of radionuclides (Bq h^{-1}) by coupling the atmospheric dispersion simulation under the assumption of a unit release rate (1Bq h^{-1}) with environmental monitoring data. In Chino et al. (2011), temporal changes in the release rates of March 15 were not estimated because some important equipment (e.g., stack monitors, radiation, and meteorological stations), which was deployed within 20 km of FNPP1 to measure air dose rates and meteorological conditions, did not work on March 15, 2011 due to the severe earthquake and/or tsunami. Afterwards, the release rates during the morning and afternoon of March 15, which formed the highest dose rate zone to the northwest of

42   FNPP1, were revised by the similar method based upon comparisons between calculated

43   and observed air dose rates from off-site monitoring posts > 20 km far from FNPP1

44   (Katata et al., 2011).

45   Because no environmental data was available, our previous paper of Chino et al.

46   (2011) did not estimate the release rates in the early phase of the FNPP1 accident, i.e.,

47   from the morning of March 12 to late at night on March 14, but they were assumed to

48   be the same as the first estimated value taken at 21:00 JST on March 14. After the

49   preliminary estimation was made, additional environmental monitoring data from

50   March 12 to 14 including dust sampling data were reported by the Tokyo Electric Power

51   Company (TEPCO) and the Ministry of Economy, Trade and Industry (METI) on May

52   28 and June 3, respectively (TEPCO, 2011a; METI, 2011a). This enables us to estimate

53   the atmospheric release during the early phase of the accident by the reverse estimation

54   method.

55   Thus, the present study aims to estimate the source terms of ^{131}I and ^{137}Cs from the

56   morning of March 12 to late at night on March 14 by coupling additional dust sampling

57   data around FNPP1 (METI, 2011a) with numerical simulations of a computer-based

58   nuclear emergency response system, WSPEEDI-II (Terada et al., 2008) under the

59   assumption of a unit release rate (1 Bq h^{-1}). A local-scale atmospheric dispersion is

60   analyzed by comparing air dose rates and surface deposition calculated by atmospheric

61   dispersion simulations using an estimated source term with observed ones from aerial

62   and ground-level monitoring. Evaluation of atmospheric release estimated by Chino et

63   al. (2011) by comparing WSPEEDI-II calculations with the data of surface deposition of

64   ^{131}I and ^{137}Cs collected from 9:00 JST on March 18, and analysis of regional-scale

65   atmospheric dispersion are described in a companion paper (Terada et al., 2011).

66

67   **2. Methods**

68   **2.1 Study area and the environmental data**

69   Atmospheric dispersion simulations were carried out for the 190-km square area in

70   Fukushima Prefecture, Japan. The site of FNPP1 is located near the Pacific coast and

71   lies on the eastern side of the Abukuma Highlands with an altitude of up to 1000 m.

72   Three computational domains are set for meteorological prediction and two inner

73   domains are used for atmospheric dispersion calculations (Katata et al., 2011). The

74   locations of dust sampling and monitoring points used in the present study are shown in

75   Fig. 1.

76   The dust sampling data from the early phase of the accident were obtained from

77   METI (METI, 2011a) and the Japan Atomic Energy Agency (JAEA, 2011a). The values

78   for the concentrations of ^{131}I, taken as the sum of both particulate and gaseous phases in

79   sampled air, are listed in Table 1. For estimation of the major release during the

80   afternoon of March 12, the measurements of air dose rate by monitoring cars from 6:00

81   to 15:00 JST on March 13 (METI, 2011a) were used because no dust sampling data

82   were available. To compare the calculated air dose rate with observed rate, the

83   equivalent gamma dose rate (Sv h^{-1}) shown in most of the data was assumed to be equal

84   to the air absorbed gamma dose rate (Gy h^{-1}). To validate the estimated source term, the

85   ground-level observations for the air dose rate in Fukushima (Fukushima Prefecture,

86   2011a, b; TEPCO, 2011b) and Ibaraki Prefectures (Ibaraki Prefecture, 2011; JAEA,

87   2011b) were used for comparison to calculations made by WSPEEDI-II.

88

89   **Table 1**

90

91   **Figure 1**

92

93   **2.2 Reverse estimation methods**

94   The reverse estimation method (Chino et al., 2011) calculates the release rates of

95   the individual radionuclides by coupling environmental monitoring data with

96   atmospheric dispersion simulations, assuming a unit release rate (1 Bq h^{-1}).

97

98   *Method 1*. Release rates are obtained as the ratio of measured to calculated air

99   concentrations of nuclide i at the sampling points, as follows:

100    $$Q_i = M_i / C_i \, ,$$ (1)

101   where Q_i is the release rate (Bq h^{-1}) of i when discharged into the atmosphere, M_i the

102   measured air concentration (Bq m^{-3}) of i, and C_i the dilution factor (h m^{-3}) of i, which is

103   equal to the air concentration calculated under the assumption of a unit release rate. This

104   method of using the data of air concentrations is more reliable than the following

105   methods described below because it does not require an assumption for the composition

106   of radionuclides.

107

108   *Method 2*. When air concentration data were not available, release rates were

109   estimated by comparing observed spatial patterns of air dose rates from radionuclides

110   on the ground surface (i.e., ground-shines) with calculated rates. This method was

111   applied to estimate the release rate during the afternoon of March 12 after the hydrogen

112   explosion occurred at Unit 1. First, the spatial pattern of the observed air dose rate due

113   to ground-shines is reproduced by WSPEEDI-II assuming a unit release rate. Then, the

114   conversion factor, which is equal to the release rate (Bq h^{-1}), is multiplied to the

115   calculated contour values so that the absolute values of the calculation become similar

116   to the measurements.

117

118   *Method 3*. When neither the dust sampling nor off-site air dose rate data were

119   obtained around FNPP1, release rates were estimated by combining the data of air dose

120   rates observed at the boundary of FNPP1, the leeward of the nuclear reactors, with

121   isopleths of those derived from the Gaussian plume model (Taki et al., 1990) under the

122   assumption of a unit release rate (1 Bq h^{-1}). This situation was found in the period from

123   7:00 to 9:30 JST on March 14. The method requires data on the wind speed, the

124   atmospheric stability, the release height, the downwind distance from the release point,

125   the effective gamma-energy of the nuclides, and the composition of the major

126   radionuclides.

127

2.3 Radionuclides

As described in the previous subsection, the compositions of the radionuclides are required for the calculation of dose rates when the data of air dose rates are used to estimated release rates. Major radioactive species of ^{131}I, ^{132}I (^{132}Te), ^{134}Cs and ^{137}Cs were considered in the calculation. Iodine-132 is treated as ^{132}Te progeny nuclide and radioactive equilibrium between ^{132}Te (half life = 3.2 d) and ^{132}I (half life = 2.3 h) is assumed (Katata et al., 2011). From 5:00 JST on March 12 to 0:00 JST on March 15, the data for the ^{137}Cs concentration were rather limited compared with ^{131}I. Thus, the fixed value of 0.1, determined from available datasets (METI, 2011a; Furuta et al., 2011), was used for the ratio of ^{137}Cs to ^{131}I for the period from 5:00 JST on March 12 to 0:00 JST on March 15. The concentration of ^{134}Cs was given to be equal to that of ^{137}Cs based on the same datasets. While the radioactive ratio of ^{132}Te to ^{131}I varied widely from 0.1 to 3 in the datasets, the overall values ranged from 1.9 to 2.5 on March 12, and later on, gradually decreased to 1.0. Considering this tendency, the ratios of ^{132}Te to ^{131}I were set to 2.0 until 16:00 JST on March 12, and 1.3 from 16:00 JST on March 12 to 21:30 JST on March 14 (see Table 3, vide infra).

9

144   In addition to the radioactivity ratio of deposited nuclides, the ratio of the

145   radioactive noble gas, ^{133}Xe, to ^{131}I is also needed for calculations using *Method 3*.

146   Because there were no available environmental data for ^{133}Xe near the site, the release

147   rate of 4.0×10^{15} Bq h^{-1} was used for ^{133}Xe, as estimated by the severe accident analysis

148   for Unit 3 of FNPP1 (JNES, 2011). Although other nuclides such as ^{136}Cs, ^{133}I, and

149   ^{129m}Te were also observed at the monitoring points in and around FNPP1 (e.g., TEPCO

150   2011c; Furuta et al. 2011), gamma air dose rates of these radionuclides calculated from

151   both air concentration data and effective energies were relatively small compared with

152   those for the major radioactive species of ^{131}I, ^{132}I (^{132}Te), ^{134}Cs, and ^{137}Cs. Thus, the

153   other radionuclides except for major species were neglected in the estimation of source

154   term.

155

156   **2.4 Atmospheric dispersion simulation**

157   WSPEEDI-II used for the atmospheric dispersion simulation includes the

158   combination of two models: a non-hydrostatic atmospheric dynamic model (MM5,

159   Grell et al., 1994) and a Lagrangian particle dispersion model (GEARN, Terada and

160   Chino, 2008). The performance of this system was evaluated by its application to the

161 field tracer experiment over Europe, ETEX (Furuno et al., 2004), Chernobyl nuclear

162 accident (Terada et al., 2004; Terada and Chino, 2005, 2008). A detailed description of

163 the models is provided in Terada et al. (2004) and Terada and Chino (2005).

164   The simulation conditions of WSPEEDI-II are summarized in Table 2. The sets of

165 calculations for one case were carried out using two sets of meteorological input data, a

166 Grid Point Value (GPV) of the Global Spectral Model for Japan region (GSM) and the

167 Meso-Scale Model (MSM) provided by the Japan Meteorological Agency (JMA).

168 Comparing the simulation results using the above two datasets, the air concentration,

169 which agreed better with observations, was used to estimate the release rates. According

170 to Katata et al. (2011), a four-dimensional data assimilation method was also employed

171 in this work using the wind data of FNPP1, Fukushima Daini Nuclear Power Plant

172 (hereinafter referred to as FNPP2) (METI, 2011b), and surface weather stations to

173 improve the prediction accuracy of the meteorological fields around FNPP1. While the

174 other settings were similar to Katata et al. (2011), calculation results for the

175 meteorological fields slightly changed in the present study because the initial and

176 boundary conditions of the meteorological input data are different.

177

178   **Table 2**

179

180   For *Method 2*, the result of the source term estimation is sensitive to the dry

181   deposition calculations. In GEARN, the amount of dry deposition of an each marker

182   particle was proportional to its radioactivity with constant values of dry deposition

183   velocity. The dry deposition velocity for ^{131}I and ^{137}Cs was set at a constant 3 and 1 mm

184   s^{-1}, respectively, for the land-use category of short vegetation in MM5. As described in

185   Katata et al. (2011), values of dry deposition velocity that were five times larger were

186   applied to the category of forests because forests have tall canopy heights and large leaf

187   surface areas that enable them to capture a large amount of radionuclides in the

188   atmosphere.

189   Most emissions were simulated as "point source" at a given release height (Table 3,

190   vide infra). The release heights were set to values of 20 and 120 m by assuming the

191   situation of leakage from the primary containment vessel (PCV) and venting at the top

192   of stack with 120 m height, respectively. The settings of the release heights for each

193   period of source term estimation are provided in Table 3. Only for hydrogen explosions

194   at Units 1 and 3, an initial three-dimensional quadrangular source of emissions was

12

195   applied. In calculations with volume source, modeled radioactive particles are uniformly

196   distributed in the volume. Based on available videos online (e.g.,

197   http://www.youtube.com/watch?v=B3_ZRO5oATk&feature=related),   the

198   three-dimensional sizes of the hydrogen explosions were assumed to be (x, y, z) = (100,

199   100, 100 m) and (100, 100, 300 m) for Units 1 and 3, respectively.

200

201   **2.5 Uncertainties in estimation methods**

202   In three methods described in subsection 2.1, *Method 1* is more accurate than other

203   two methods. *Method 1* has errors that mainly arise due to the atmospheric dispersion

204   simulation and dust sampling data. In contrast, for *Methods 2* and *3*, the uncertainty in

205   the radioactivity ratio may cause significant errors in the source term estimation, as

206   described in subsection 2.1. In addition, these two methods also have potential errors

207   that are as described below.

208   In *Method 2*, the maximum value of the observed air dose rate is assumed to be 30

209   μGy h^{-1}, which is the upper limit of measurable dose of the NaI (Tl) scintillation counter.

210   Although the air dose rate higher than 30 μGy h^{-1} can be usually observed by the

211   ionization chamber at the monitoring posts in and around FNPP1 (Fig. 2c, 6, and 7), this

212   instrument was unfortunately not used during the period when the *Method 2* was applied.

213   By comparing the value with that of contours calculated by WSPEEDI-II, the release

214   rate is estimated in this method. Therefore, if the real value of the observed air dose rate

215   was greater than 30 μGy h^{-1}, the release rate would be underestimated. The method has

216   also an uncertainty due to the dry deposition velocity in the calculations. From the

217   literature, the values of dry deposition velocity for ^{131}I and ^{137}Cs vary by more than one

218   order of magnitude (Brandt et al., 2002). This variation in dry deposition velocity

219   directly affects the estimation result of the release rate because calculated and observed

220   air dose rates due to ground-shines were compared to each other by this method.

221   For *Method 3*, there are also two uncertainties due to the release rate of ^{133}Xe and

222   observed wind direction with a low accuracy (16-sectors). If no release of ^{133}Xe is

223   assumed to evaluate the situation where other major radionuclides are dominant, the

224   estimated release rate of ^{131}I could be double that of when the release rate of ^{133}Xe was

225   4.0×10^{15} Bq h^{-1} (subsection 2.3). With regard to wind direction, in principle, the

226   measured value has errors of $\pm 11.25°$ due to the number of sectors being 16. If the

227   angle of the principal axis of the plume increases or decreases by 11.25° according to

228   the wind direction, the estimated release rate of ^{131}I can be 6 times as large as the one

229   when the principal axis is assumed to be along the monitoring post.

230   Therefore, in terms of accuracy of estimation, it should be better to use *Method 1*

231   throughout the period of the source term estimation. However, as described in

232   subsection 2.1, unfortunately *Methods 2* and *3* had to be adopted for the period when no

233   dust sampling data was available.

234

235   **3.   Results of source term estimation**

236   Temporal changes in wind speed and direction, and air dose rates observed by

237   monitoring cars around the monitoring posts (hereafter referred to as MPs), the gates,

238   and the gym on/near the border of the site of FNPP1 are illustrated in Fig. 2. The map of

239   monitoring points in FNPP1 is also depicted in Fig. 3 (TEPCO 2011d, reconstructed by

240   the authors). The release was assumed to start at 5:00 JST on March 12, just before the

241   increases in air dose rate at the main gate and near MP8 in FNPP1 (No. 1, Fig. 2c) were

242   observed. In the present study, release rates for the six periods from 5:00 JST on March

243   12 to 0:00 JST on March 15 (Nos. 1–5 and 8, Fig. 2c) were estimated from

244   environmental data. Four of them (Nos. 1, 2, 4, and 8, Fig. 2c) were estimated by

245   comparing dust sampling data with calculation results. The estimation methods based on

246   the air dose rates in and around FNPP1 were applied to the remainder of the periods

247   (Nos. 3 and 5, Fig. 2c) because no dust sampling data was available. Following our

248   preliminary study (Chino et al., 2011), the release duration was determined from

249   assuming that the release with a certain release rate continued from/to the middle

250   periods between released times of sampled air. The value of 30 min was assumed to the

251   release duration for hydrogen explosions at Units 1 and 3, as explained below.

252

253   **Figure 2**

254

255   **Figure 3**

256

257   The results of the estimated release rates of ^{131}I from 5:00 JST on March 12 to 0:00

258   JST on March 17 are summarized in Table 3. Figure 4 shows the temporal variation of

259   estimated release rates of ^{131}I and ^{137}Cs during this period. Some values of release rates

260   estimated by our past studies of Chino et al. (2011) (Nos. 7, 9, and 13, Table 3) and

261   Katata et al. (2011) (Nos. 10–12, Table 3) are included in the table and the figure. The

262   major releases of ^{131}I greater than 10^{15} Bq h^{-1} were estimated during the afternoon on

16

263   March 12 after the hydrogen explosion at Unit 1 (No. 3, Table 3) and late at night on

264   March 14 (No. 8, Table 3). The possible major release during the hydrogen explosion of

265   Unit 3 at 11:00 JST on March 14 could not be estimated because the plume flowed to

266   the Pacific Ocean on the northwesterly wind (open circle with No. 6, Fig. 2b). Thus, the

267   same value of release rate estimated for the hydrogen explosion of Unit 1 (i.e., $3.0 \times$

268   10^{15} Bq h^{-1}) was assumed for this period (No. 6, Table 3). For other time periods before

269   21:30 JST on 14 March (Nos. 1, 2, 4, 5, and 7, Table 3), estimated release rates of ^{131}I

270   had a value of 1.7×10^{13} to 8.4×10^{13} Bq h^{-1}, which was similar to our preliminary

271   estimated value (No. 7, Table 3).

272

273   **Table 3**

274

275   **Figure 4**

276

277   **3.1 Event Nos. 1–3 on March 12, 2011**

278   From the morning to the afternoon of March 12, two values of release rate of ^{131}I

279   were estimated as 3.7×10^{13} (No. 1, Table 3) and 1.7×10^{13} Bq h^{-1} (No. 2, Table 3)

17

280   using dust sampling data taken at Takase and Kawazoe, respectively (METI, 2011a).

281   The major release was then suggested by the large increases in air dose rate observed

282   near MP4, located northwest of FNPP1, soon after the hydrogen explosion of Unit 1 at

283   15:30 JST (No. 3, Fig. 2c). The fact that the air dose rates also rose up to 20 μGy h^{-1} at

284   Minami-soma, located 24 km north-northwest of FNPP1, 4.5 h after the explosion

285   (Fukushima Prefecture, 2011b) implies that the high-concentration plume passed over

286   the north-northwest region from FNPP1 during the evening of March 12. Since no dust

287   sampling data was available during this period, the release rate was estimated by

288   *Method 2* based on comparisons of the spatial patterns of observed and calculated air

289   dose rates due to ground-shines in the region in the afternoon of March 13 (Fig. 5). It

290   can be seen that the model generally reproduced the spatial distribution of observed air

291   dose rates to the north-northwest direction of FNPP1. By multiplying 3.0×10^{15} to the

292   maximum value of contours in calculation results assuming a unit release rate ($1.0 \times$

293   10^{-14} μGy h^{-1}), the calculated air dose rate becomes similar to the observed one as 30

294   μGy h^{-1}, representing the upper measurable limit of the instrument (subsection 2.5).

295   Thus, the release rate was estimated as 3.0×10^{15} Bq h^{-1} (No. 3, Table 3). The release

296   duration of the hydrogen explosion at Unit 1 was assumed to be 30 min because the

18

297   increase in air dose rate continued for approximately 30 to 60 min at MP4 (open circle

298   with No. 3 in Fig. 2c). This assumption was also expected from the fact that the high air

299   dose rates when the plume passed through continued to be observed at Minami-soma for

300   60 min (Fukushima Prefecture, 2011b).

301

302   **Figure 5**

303

304   **3.2 Event No. 4 on March 12–13, 2011**

305   The release rate of ^{131}I at 13:00 JST on March 13 was estimated as 8.4×10^{13} using

306   the dust sampling data (METI, 2011a) and was assumed to continue from 16:00 JST on

307   March 12 to 23:00 JST on March 13 (No. 4, Fig. 2c and Table 3).

308

309   **3.3 Event Nos. 5–7 on March 14, 2011**

310   At 9:00 JST on March 14 (No. 5, Fig. 2c), *Method 3*, using a Gaussian plume

311   model, was employed because no off-site environmental data was obtained. Since the

312   southeasterly and south-southeasterly winds were frequently observed around the time,

313   the estimation was made by assuming that MP3, located northwest of Unit 3, was along

314   the center of the plume (ellipses with No. 5, Fig. 2b, c). The value of 255 μGy h^{-1},

315   formed by subtracting the minimum value of the air dose rate before the peak appeared

316   at MP3 (263 μGy h^{-1} at 8:10 JST) from the peak one (518 μGy h^{-1} at 9:11 JST,

317   downward arrow with No. 5, Fig. 2c), was used for estimation. The release rate of ^{131}I

318   from 23:00 JST on March 13 to 11:00 JST on March 14 was 3.6×10^{13} Bq h^{-1} (No. 5,

319   Table 3), under low wind speed (0.6 m s^{-1}) and stable atmospheric conditions based on

320   measurements in and around FNPP1. The release rates from 11:00 to 21:30 JST on

321   March 14 (Nos. 6–7, Fig. 2c) were assumed to be the same as Event No. 3 and were

322   taken from our preliminary results (Chino et al., 2011), as described above.

323

324   **3.4 Event No. 8 on March 14–15**

325   The release rate of ^{131}I after the increase of air dose rate at the main gate of FNPP1

326   late at night on March 15 (No. 8, Fig. 2c) was estimated as 1.3×10^{15} Bq h^{-1} using the

327   dust sampling data at JAEA. The value was estimated to have decreased to 3.5×10^{14}

328   Bq h^{-1} at 0:00 JST on March 15 estimated by the authors at the same location (Chino et

329   al., 2011; No. 9, Table 3).

330

4. Analysis of local-scale atmospheric dispersion from March 12–17

4.1 Air dose rate

Calculated air dose rates by WSPEEDI-II using the input data of MSM and estimated release rates were compared with observed rates from the ground-level and aerial monitoring. Figure 6 and Movie 1 show the spatial distributions of calculated and measured air dose rates from March 12–17. The plume moves with rainfall intensity is shown in Movie 2. As described in section 3, the source term estimated in this paper included the events of major releases ($> 10^{15}$ Bq h^{-1}) during the afternoon of March 12 and late at night on March 14, which did not appear in our previous work, Chino et al. (2011). Those releases significantly increased the amount of dry deposition, resulting in increasing air dose rate along the routes of the plume, north-northwest and south-southwest of FNPP1 (Figs. 6b–d). It should be noted that no rainfall was observed in the area until the afternoon on March 15. In the figure and movies, overall, the increases in air dose rates at the monitoring posts during and after the plume passed through were reproduced by the calculations.

The movement of the simulated plume from March 12 to 17 is explained as follows. The plume firstly flowed to the ocean until the early morning of March 12 (Fig.

21

348 6a). After the hydrogen explosion occurred at Unit 1 at 15:30 JST on March 12, the

349 high-concentration plume flowed from FNPP1 in a north-northwest direction and air

350 dose rates around the monitoring post of Minami-soma increased (Fig. 6b). The plume

351 was then carried by a southwesterly wind and flowed over the Pacific Ocean. From

352 March 13 to 14, due to the westerly wind, the plume mainly faced the ocean. The wind

353 direction changed clockwise late at night on March 14, and the high-concentration

354 plume dispersed to the south-southwest direction of FNPP1 (Fig. 6c). The air dose rates

355 rose in order of the monitoring posts at FNPP2, Iwaki, Kitaibaraki, and Tokai with the

356 pass of the plume. According to the ground-level monitoring (MEXT 2011b), the plume

357 dispersed on the northerly and north-easterly winds and caused surface deposition over

358 wide areas of East Japan (Terada et al., 2011, the companion paper). Then, the

359 high-concentration plume again changed its direction clockwise and flowed to the

360 southwest (Fig. 6d) and the northwest of FNPP1 (Fig. 6e). As shown in the simulation

361 results of Katata et al. (2011), the plume encountered a band of rain that caused wet

362 deposition in the areas around Koriyama, Iitate, and Fukushima. On the early morning

363 on March 16, the wind changed from southeasterly to northwesterly and the plume

364 flowed to the ocean through the coast of FNPP1 until the end of the simulation (Fig. 6f).

22

365

366   **Figure 6**

367

368   Figure 7 depicts the comparison between measured and calculated air dose rates at

369   several monitoring points in Fukushima and Ibaraki prefectures. It should be noted that

370   the calculations at the location to the 7 km west of Minami-soma was used for the

371   comparisons in Fig. 7d in order to adjust the distance of the principal axes of the

372   high-concentration plume discharged immediately after the hydrogen explosion at Unit

373   1 between calculations and observations at the latitude of Minami-soma (Fig. 5). The

374   calculations for air dose rates slightly differ from those shown in Katata et al. (2011)

375   because the initial and boundary conditions of meteorological input data are different.

376   Figure 7 shows that increases of observed air dose rates due to ground-shines were

377   generally reproduced by the model, while some discrepancies were found in

378   calculations at Fukushima (Fig. 7a) and several locations to the south-southwest

379   direction of FNPP1 (Figs. 7e–h). These discrepancies between observations and

380   calculations may be due to the errors in wind and precipitation fields predicted by the

381   model.

382

383   **Figure 7**

384

385   **4.2 Surface deposition of ^{137}Cs**

386   Figure 8a shows the distribution map for the surface deposition of ^{137}Cs

387   accumulated over the whole simulation period. Overall, the calculated distribution

388   pattern of surface deposition around FNPP1 agreed with the observed one by combining

389   airborne and ground-level monitoring (MEXT, 2011a). As described in Katata et al.

390   (2011), the areas where there was a large amount of surface deposition, southwest and

391   northwest regions of FNPP1, correspond to those due to two major releases during the

392   morning and afternoon on March 15, respectively (Fig. 8d). By calculations, the

393   high-concentration plume discharged during the hydrogen explosion at Unit 1 on March

394   12 also caused a large amount of dry deposition in the north-northwest region of FNPP1

395   (Fig. 8b). Although the route of the plume was partially overlapped with that discharged

396   during the afternoon of March 15, the former has a smaller amount of surface deposition

397   than the latter (Fig. 8d). This is because the duration of the major release on March 12

398   was short (i.e., 30 min) compared with that during the afternoon on March 15 (No. 3

399   and 12, Table 3). To the south-southwest direction from the site, a large amount of dry

400   deposition appeared near FNPP1 due to the high-concentration plumes discharged from

401   the night of March 14 to the morning of March 15 (Fig. 8c). This indicates that the air

402   dose rate significantly increased in the south-southwest area of FNPP1 by dry

403   deposition of the high-concentration plume discharged from the night of March 14 to

404   the morning of March 15. In the area around Iwaki and Kitaibaraki, the accumulated

405   surface deposition of ^{137}Cs until 9:00 JST on March 16 (Fig. 8a) was smaller than that

406   reported by airborne monitoring after July 22 (MEXT 2011a). This difference between

407   calculations and observations can be explained by the additional surface deposition after

408   9:00 JST on March 16. From atmospheric dispersion simulations of eastern Japan from

409   March 12 to May 1 (Terada et al., 2011, the companion paper) and measurements of air

410   dose rates in Fukushima and Ibaraki Prefectures (Fig. 7), surface deposition of ^{137}Cs

411   also occurred due to wet deposition in the area around noon on March 16 and from

412   March 21 to 23.

413

414   **Figure 8**

415

5. Conclusion

The source term of ^{131}I and ^{137}Cs in the early phase of the FNPP1 accident from March 12 to 14 was estimated by combining environmental data with atmospheric dispersion simulations of a computer-based nuclear emergency response system, WSPEEDI-II under the assumption of a unit release rate (1Bq h^{-1}). Major releases, greater than 10^{15} Bq h^{-1} for ^{131}I, were estimated during the afternoon of March 12 after the hydrogen explosion at Unit 1 and late at night on March 14. The release rate in other periods, from 5:00 JST on March 12 to 0:00 JST on March 15, were on the order of 10^{13} Bq h^{-1}, which was similar to the preliminary estimated value in the previous paper presented by the authors. The release rate of the hydrogen explosion at Unit 3 on March 14 could not be estimated due to the lack of environmental data. The spatial pattern of surface deposition of ^{137}Cs and increases in air dose rates observed at the monitoring posts around FNPP1 were generally reproduced by WSPEEDI-II using estimated release rates. The simulation results indicate that the amount of dry deposition of the high-concentration plume discharged during the afternoon of March 12 was clearly smaller than that of the total deposition from the afternoon to the evening of March 15, which formed the highest dose rate zone in the northwest region of FNPP1. The results

433   indicate that air dose rates largely increased in the south-southwest region of the site by

434   dry deposition of the high-concentration plume discharged from the night of March 14

435   to the morning of March 15.

436

445

446   **References**

447   Brandt, J., Christensen, J.H., Frohn, L.M., 2002. Modelling transport and deposition of

448   caesium and iodine from the Chernobyl accident using the DREAM model. Atmos.

449   Chem. Phys., 2, 397-417.

450

451   Chino, M., Nakayama, H., Nagai, H., Terada, H., Katata, G., Yamazawa, H., 2011.

452   Preliminary estimation of release amounts of ^{131}I and ^{137}Cs accidentally discharged from

453   the Fukushima Daiichi nuclear power plant into atmosphere. J. Nucl. Sci. Technol., 48,

454   1129-1134.

455

456   Fukushima Prefecture, 2011a.

457   <http://www.pref.fukushima.jp/j/20-50km0315-0331.pdf> (in Japanese, accessed 18

458   November 2011).

459

460   Fukushima Prefecture, 2011b. <http://www.pref.fukushima.jp/j/7houbu0311-0331.pdf>

461   (in Japanese, accessed 18 November 2011).

462

463   Furuno, A., Terada, H., Chino, M., Yamazawa, H., 2004. Experimental verification for

464   real-time environmental emergency response system: WSPEEDI by European tracer

465   experiment. Atmos. Environ., 38, 6989-6998.

466

467   Furuta, S., Sumiya, S. Watanabe, H. Nakano, M., Imaizumi, K., Takeyasu, M., Nakada,

468   A., Fujita, H., Mizutani, T., Morisawa, M., Kokubun, Y., Kono, T., Nagaoka, M.,

469   Yokoyama, H., Hokama, T., Isozaki, T., Nemoto, M., Hiyama, Y., Onuma, T., Kato, C.,

470   Kurachi, T., 2011. Results of the Environmental Radiation Monitoring Following the

471   Accident at the Fukushima Daiichi Nuclear Power Plant. JAEA-Review 2011-035,

472   JAEA, in press (in Japanese with English abstract, available online).

473

474   Grell, G.A., Dudhia, J., Stauffer, D.R., 1994. A description of the fifth-generation Penn

475   State/NCAR Mesoscale Model (MM5). NCAR Tech. Note NCAR/TN-3921STR, 122

476   pp.

477

478   Ibaraki Prefecture, 2011. <http://www.pref.ibaraki.jp/20110311eq/radiation.html> (in

479   Japanese, accessed 18 November 2011).

480

481   JAEA, Japan Atomic Energy Agency, Nuclear Emergency Assistance and Training

482   Center, 2011a. Personal communication.

483

484   JAEA, 2011b. Transition of radiation rates measured at environmental monitoring posts

485   of the sites of JAEA

486   <http://www.jaea.go.jp/english/jishin/e-monitor.pdf> (accessed 18 November 2011).

487

488   JNES, Japan Nuclear Energy Safety Organization, 2011. JNES-RE-2011-0002,

489   JNES-RE-Report Series. <http://www.jnes.go.jp/content/000119740.pdf> (in Japanese,

490   accessed 18 November 2011).

491

492   Katata, G., Terada, H., Nagai, H., Chino, M., 2011. Numerical reconstruction of high

493   dose rate zones due to the Fukushima Daiichi Nuclear Power Plant accident. J. Environ.

494   Radioact., in press (doi:10.1016/j.jenvrad.2011.09.011).

495

496   METI, Ministry of Economy, Trade and Industry, 2011a.

497   <http://www.meti.go.jp/press/2011/06/20110603019/20110603019.html> (in Japanese,

498   accessed 18 November 2011).

499

500   METI, 2011b. <http://www.meti.go.jp/press/20110316001/20110316001-2.pdf> (in

501   Japanese, accessed 18 November 2011).

502

503   MEXT, Ministry of Education, Culture, Sports Science and Technology, 2011a. MEXT

504   and DOE Airborne Monitoring

505   <http://radioactivity.mext.go.jp/en/monitoring_around_FukushimaNPP_MEXT_DOE_a

506   irborne_monitoring/> (accessed 18 November 2011).

507

508   MEXT, 2011b. Reading of environmental radioactivity level by prefecture (March

509   2011)

510   <http://radioactivity.mext.go.jp/en/monitoring_by_prefecture/2011/03/index.html>

511   (accessed 18 November 2011).

512

513   Prime Minister of Japan and His Cabinet, 2011. Report of Japanese Government to the

514   IAEA Ministerial Conference on Nuclear Safety - The Accident at TEPCO's Fukushima

515   Nuclear Power Stations

516   <http://www.kantei.go.jp/foreign/kan/topics/201106/iaea_houkokusho_e.html#top>

517   (accessed 18 November 2011).

518

519   Taki, M., Kobayashi, H., Suzuki, T., Shimizu, I., 1990. Isopleths if surface air

520   concentration and surface air absorbed dose rate due to a radioactive cloud released

521   from a stack. JAERI-M-90-206 (in Japanese with English abstract).

522

523   TEPCO, Tokyo Electric Power Company, 2011a. Additional monitoring data at

524   Fukushima Daiichi Nuclear Power Station

525   <http://www.tepco.co.jp/en/press/corp-com/release/11052811-e.html>   (accessed   18

526   November 2011).

527

528   TEPCO, 2011b. Radiation dose measured in the Fukushima Daini Nuclear Power

529   Station   <http://www.tepco.co.jp/en/nu/fukushima-np/f2/index-e.html>   (accessed   18

530   November 2011).

531

532   TEPCO, 2011c. Influence to surrounding environment, Archives

533   <http://www.tepco.co.jp/en/nu/fukushima-np/f1/index2-e.html> (accessed 18 November

534   2011).

535

536   TEPCO, 2011d. Radiation dose measured in the Fukushima Daiichi Nuclear Power

537   Station <http://www.tepco.co.jp/en/nu/fukushima-np/f1/index-e.html> (accessed 18

538   November 2011).

539

540   Terada, H., Chino, M., 2005. Improvement of Worldwide Version of System for

541   Prediction of Environmental Emergency Dose Information (WSPEEDI), (II) Evaluation

542   of numerical models by ^{137}Cs deposition due to the Chernobyl nuclear accident. J. Nucl.

543   Sci. Technol., 42, 651-660.

544

545   Terada, H., Chino, M., 2008. Development of an atmospheric dispersion model for

546   accidental discharge of radionuclides with the function of simultaneous prediction for

547   multiple domains and its evaluation by application to the Chernobyl nuclear accident. J.

548   Nucl. Sci. Technol., 45, 920-931.

549

550   Terada, H., Furuno, A., Chino, M., 2004. Improvement of Worldwide Version of System

551   for Prediction of Environmental Emergency Dose Information (WSPEEDI), (I) New

552 combination of models, atmospheric dynamic model MM5 and particle random walk

553 model GEARN-new. J. Nucl. Sci. Technol., 41, 632-640.

554

555 Terada, H., Katata, G., Chino, M., Nagai, H., 2011. Atmospheric discharge and

556 dispersion of radionuclides during the Fukushima Daiichi Nuclear Power Plant accident.

557 Part II: Verification of the source term and regional-scale atmospheric dispersion. J.

558 Environ. Radioact., submitted (the companion paper).

559

560 Terada, H., Nagai, H., Furuno, A., Kakefuda, T., Harayama, T., Chino, M., 2008.

561 Development of Worldwide version of system for prediction of environmental

562 emergency dose information: WSPEEDI 2nd version. Trans. At. Energy Soc. Japan., 7,

563 257-267 (in Japanese with English abstract).

564

SUPPLEMENTARY MOVIE CAPTIONS

565

566

567 **Movie 1** Simulated spatial distributions of air dose rate (shaded areas, μGy h^{-1}) from

568 5:00 JST on March 12 to 0:00 JST on March 17, 2011. Values and colors of circles in

569 the figures represent observed air dose rates at monitoring posts.

570

571 **Movie 2** Simulated spatial distributions of vertically accumulated concentration of ^{131}I

572 (red contours, Bq m^{-3}) and rainfall intensity (shaded areas, mm h^{-1}) from 5:00 JST on

573 March 12 to 0:00 JST on March 17, 2011.

574

FIGURE CAPTIONS

576

577 **Figure 1.**

578 Environmental monitoring points used in the present study from 5:00 JST on March 12

579 to 0:00 JST on March 17, 2011.

580

581 **Figure 2.**

582 (a) Wind speed, (b) wind direction, and (c) air dose rates observed around monitoring

583 posts (MP) at the FNPP1 from March 12 to 16, 2011 (TEPCO, 2011a). Words in

584 parentheses show the rough directions of the monitoring points from the nuclear

585 reactors (see Fig. 3). Numbers denoted in figures and arrows in (c) represent the

586 numbers of the estimation and release duration listed in Table 1.

587

588 **Figure 3.**

589 Map of monitoring points in FNPP1 (TEPCO 2011d, reconstructed by the authors).

590

591 **Figure 4.**

592 Temporal changes of estimated release rates of ^{131}I and ^{137}Cs from March 12 to 17, 2011.

593 The open circles represent the released time of sampled air for ^{131}I shown in Table 3.

594 Thin lines show prior estimations of Chino et al. (2011) and Katata et al. (2011). The

595 date and time of important plant events (Prime Minister of Japan and His Cabinet, 2011)

596 are also shown in the figure.

597

598 **Figure 5.**

599 Comparison of air dose rates in the north-northwest area of the FNPP1 between

600 measurements from 6:00 to 15:00 JST and calculations at 12:00 JST on March 13, 2011.

601 Dashed straight represent the main axes of observed and calculated plumes. As shown

602 in the horizontal arrow between two dashed lines, the principal axis of the calculated

603 plume seemed to be approximately 7 km further west from that of the observed axis at

604 the latitude of the monitoring post of Minamisoma (see subsection 4.1).

605

606 **Figure 6.**

607 Simulated spatial distributions of air dose rate from March 12 to 16, 2011. Values and

608 colors of circles in the figures represent observed air dose rates at monitoring posts. The

609 minimum significant digit is 0.01, which was determined from the observational data of

610   air dose rates.

611

612   **Figure 7.**

613   Temporal changes in calculated (lines) and observed (circles) air dose rates at the

614   several monitoring posts shown in Fig. 1. Note that the calculations at the location 7 km

615   west of Minamisoma was used for comparisons in (d) in order to adjust the distance of

616   principal axes of the high-concentration plume discharged immediately after the

617   hydrogen explosion at Unit 1 between calculations and observations at the latitude of

618   Minamisoma (Fig. 5).

619

620   **Figure 8.**

621   Spatial distributions of accumulated surface deposition of ^{137}Cs (a) during the whole

622   simulation period, (b) from 9:00 JST on March 12 to 9:00 JST on March 13, 2011, (c)

623   from 9:00 JST on March 14 to 9:00 JST on March 15, 2011, and (d) from 9:00 JST on

624   March 15 to 9:00 JST on March 16, 2011.

625

626

FIGURE 1

☆ Fukushima Daiichi Nuclear Power Plant (FNPP1)

○ Monitoring posts   ▲ Dust sampling points

Data code	Sampling location
a	Takase
b	Kawazoe
c	Otabashi
d	Tokai (JAEA)
e	Fukushima
f	Iitate
g	Minami-soma
h	Koriyama
i	FNPP2
j	Iwaki
k	Kitaibaraki
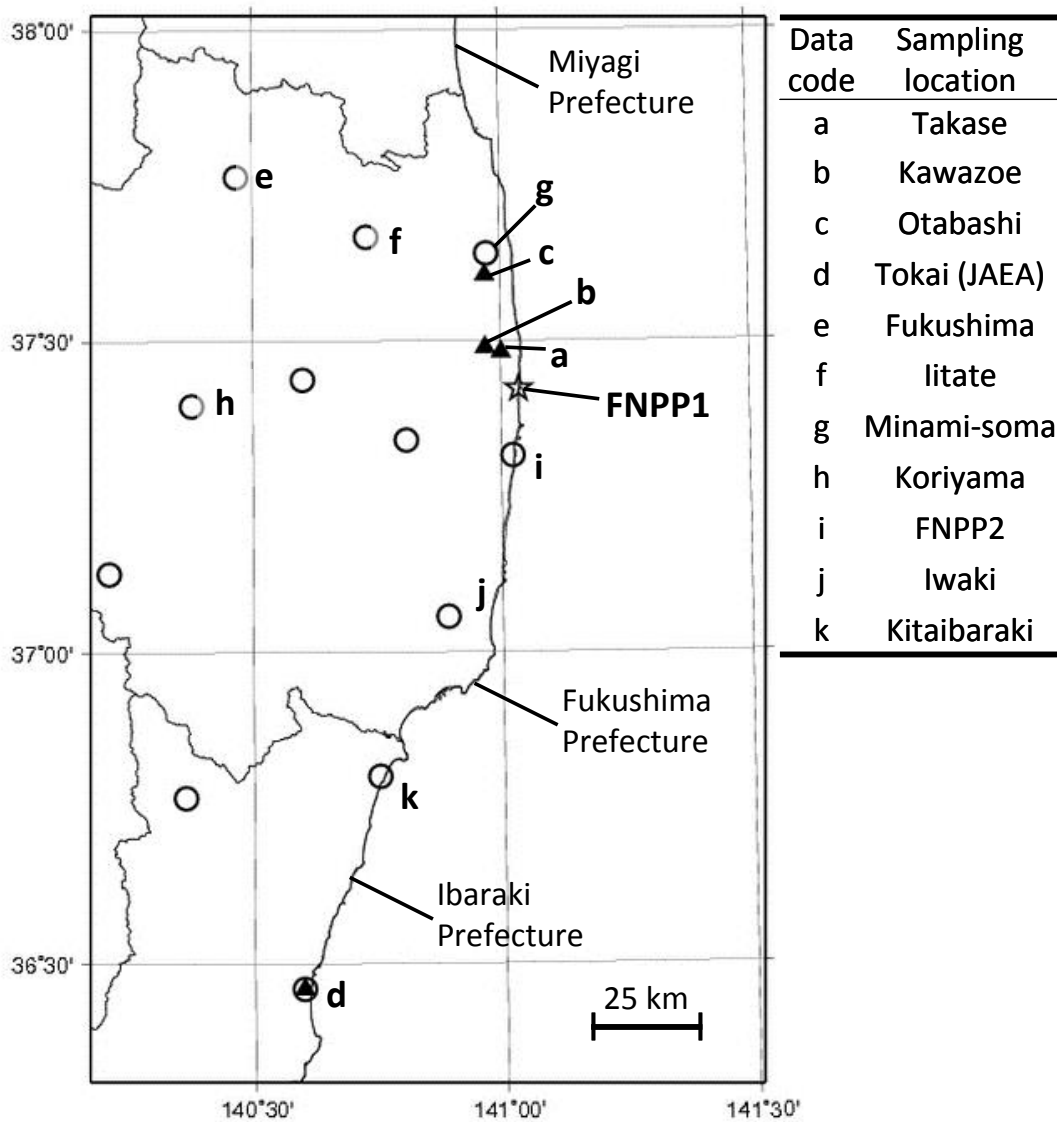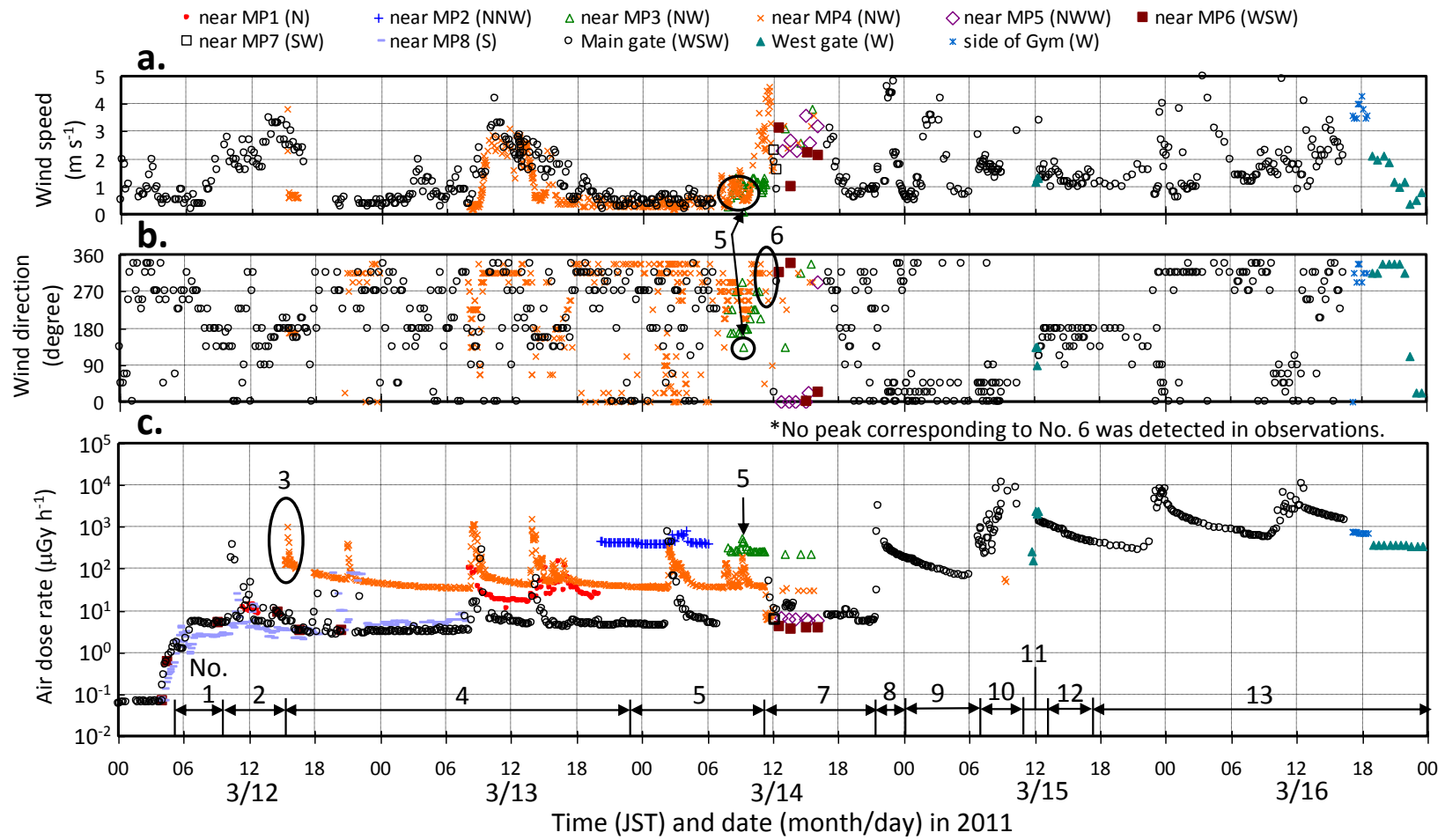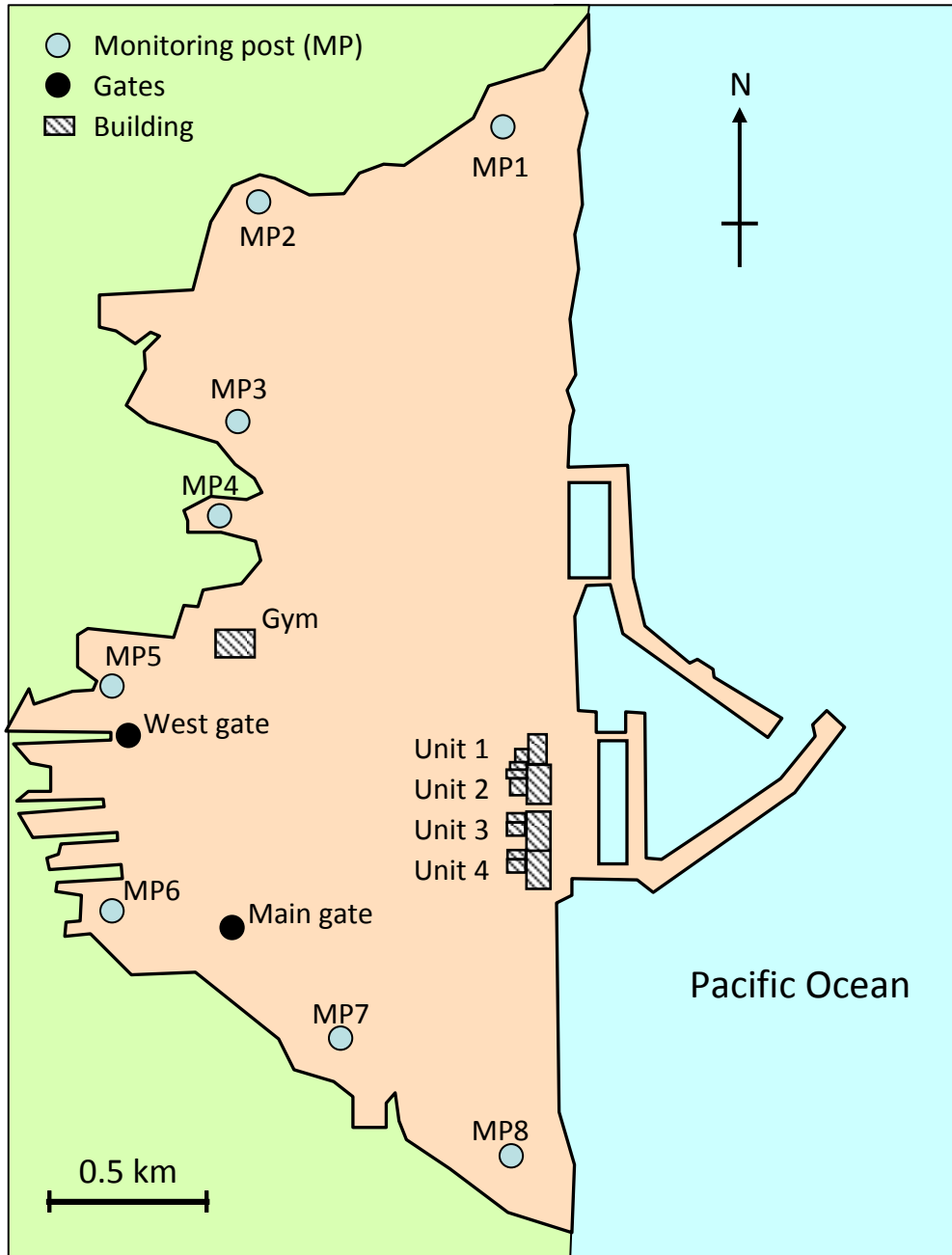
FIGURE 2

FIGURE 3

635 **FIGURE 4**

636

637

638

FIGURE 5

☆ Fukushima Daiichi Nuclear Power Plant (FNPP1)

FIGURE 6
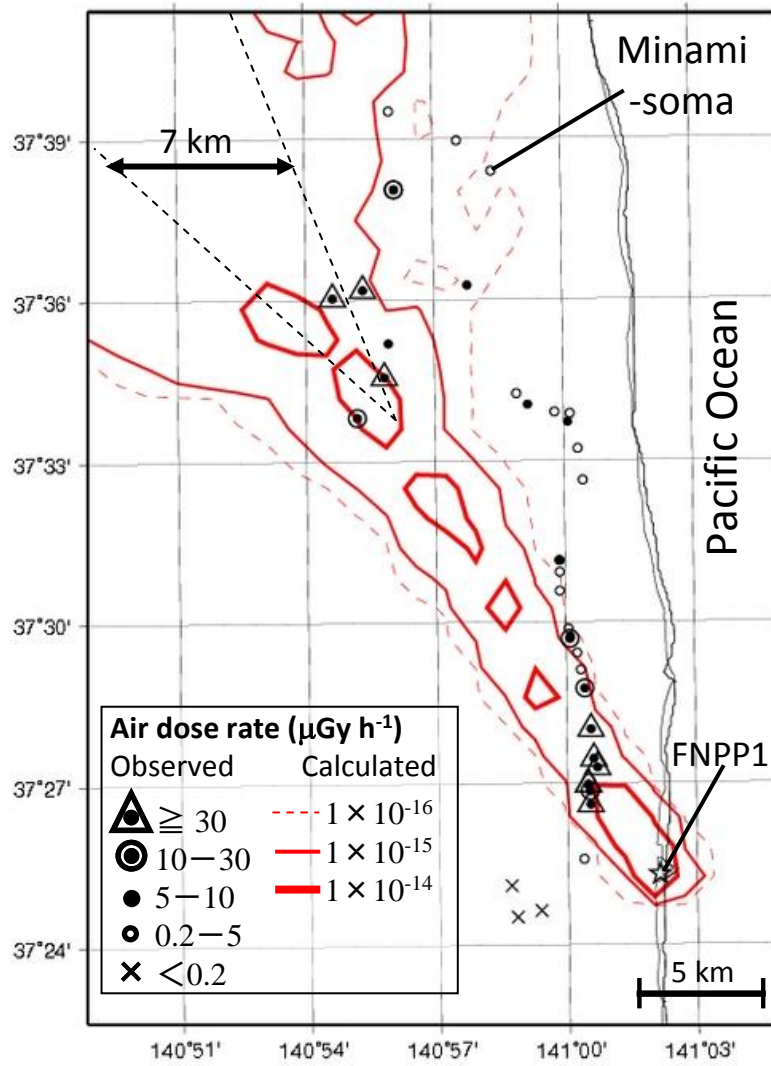
☆ Fukushima Daiichi Nuclear Power Plant (FNPP1)
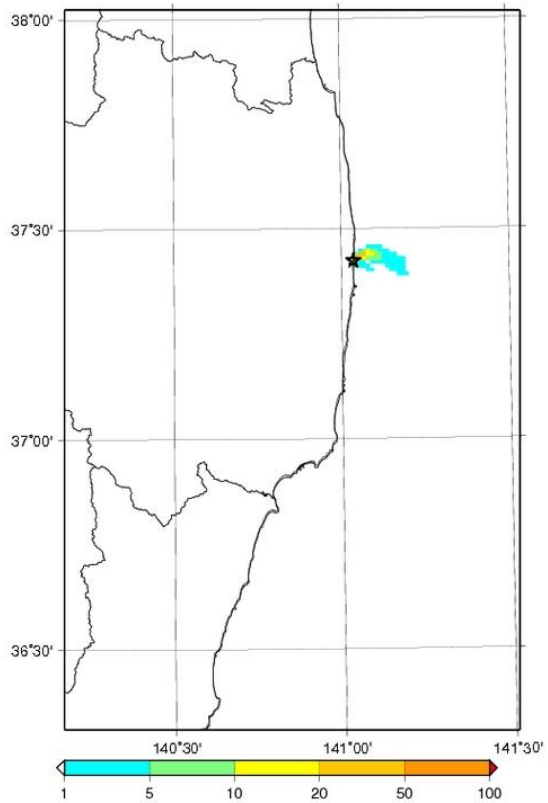
a. 9 JST on March 12   **b.** 21 JST on March 12   **c.** 9 JST on March 15
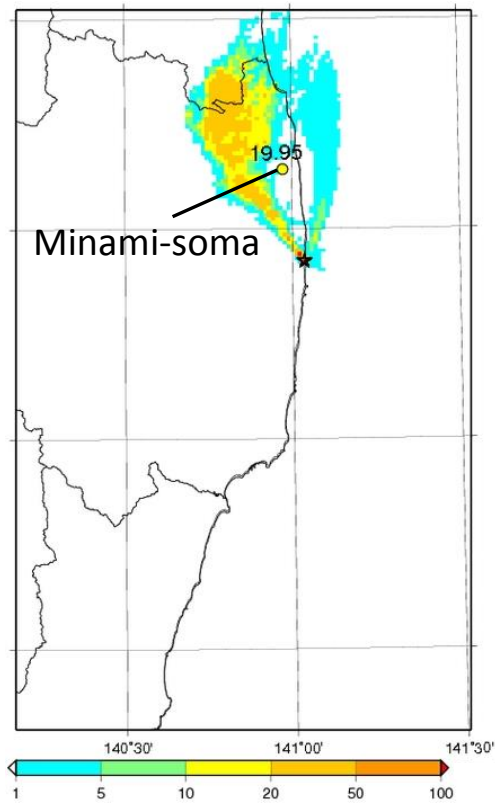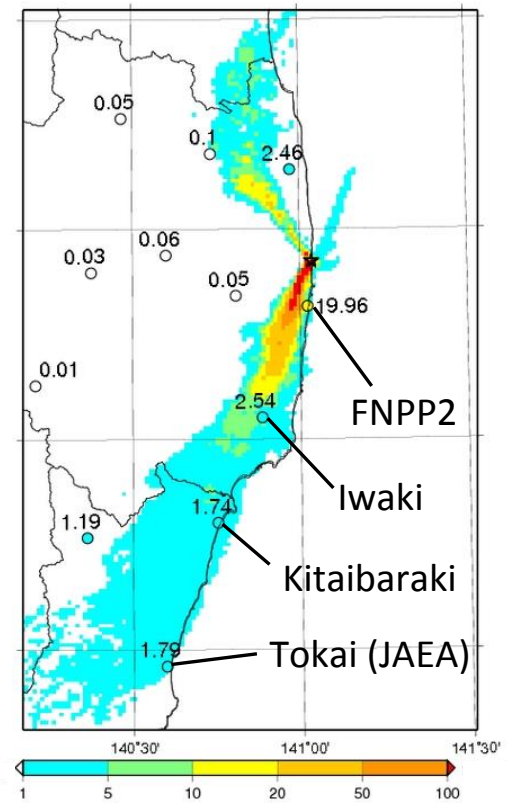
*Color shaded areas: air dose rate (μGy h^{-1})
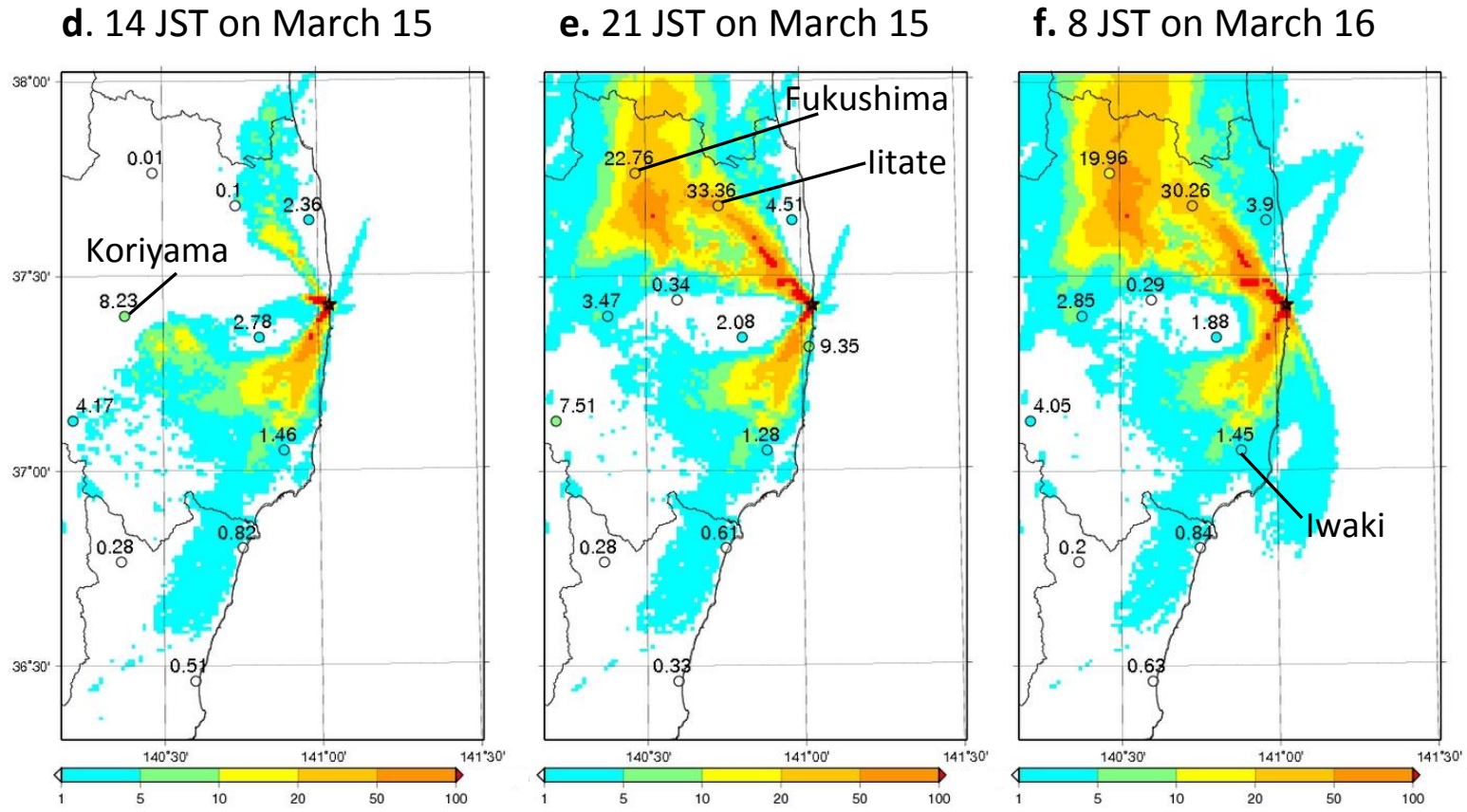
643

644

645   **FIGURE 6** (continued)

☆ Fukushima Daiichi Nuclear Power Plant (FNPP1)

d. 14 JST on March 15   **e.** 21 JST on March 15   **f.** 8 JST on March 16

*Color shaded areas: air dose rate (μGy h⁻¹)

646

44

647 **FIGURE 7**

a. Fukushima

b. Iitate

c. Koriyama

d. Minami-soma

e. Fukushima Daini Nuclear Power Plant

f. Iwaki

g. Kitaibaraki

h. Tokai (JAEA)

648
649

45

FIGURE 8
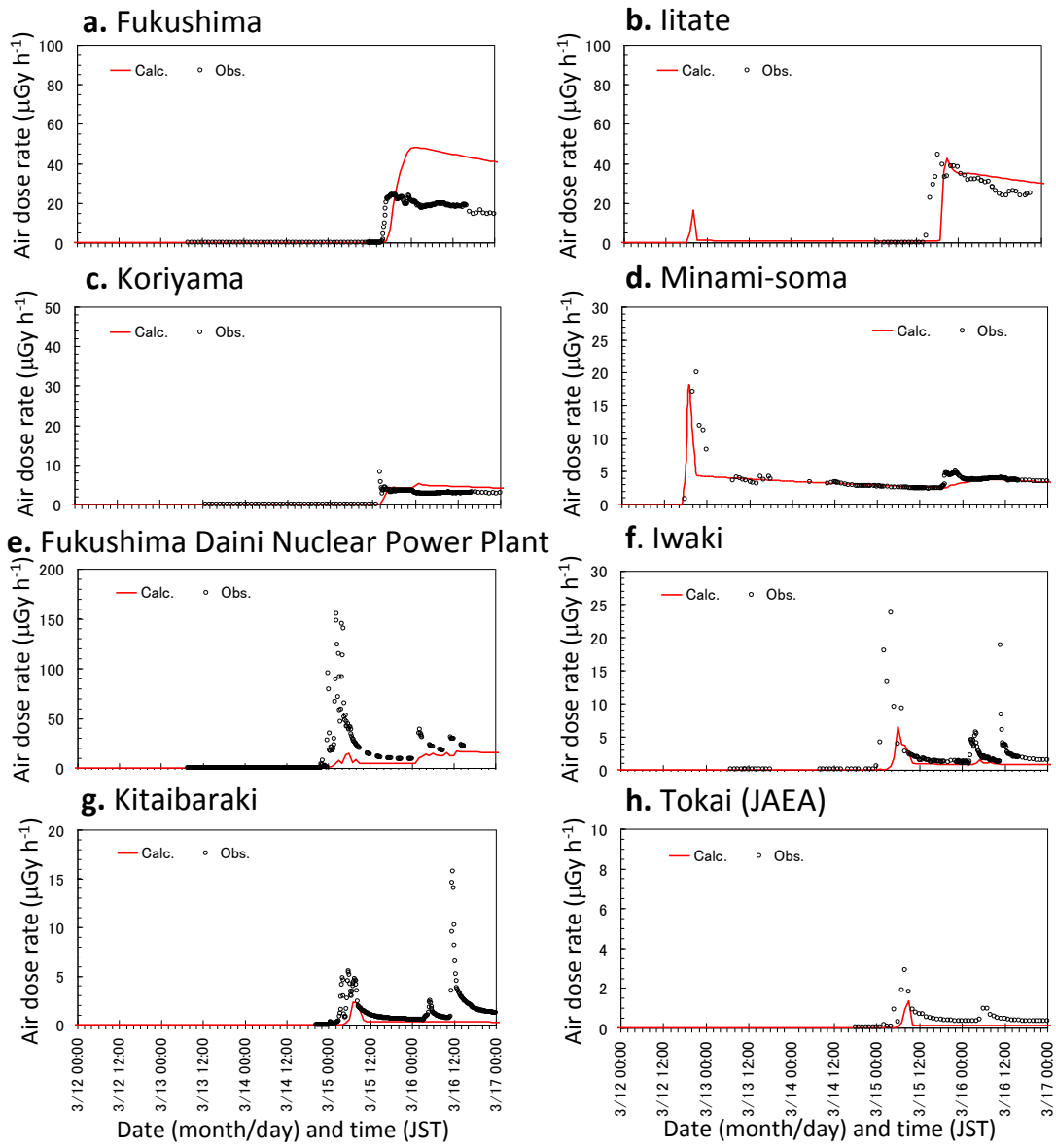
☆ Fukushima Daiichi Nuclear Power Plant (FNPP1)

a. Total deposition to 3/17 0 JST   **b**. 3/12 9 JST －3/13 9 JST
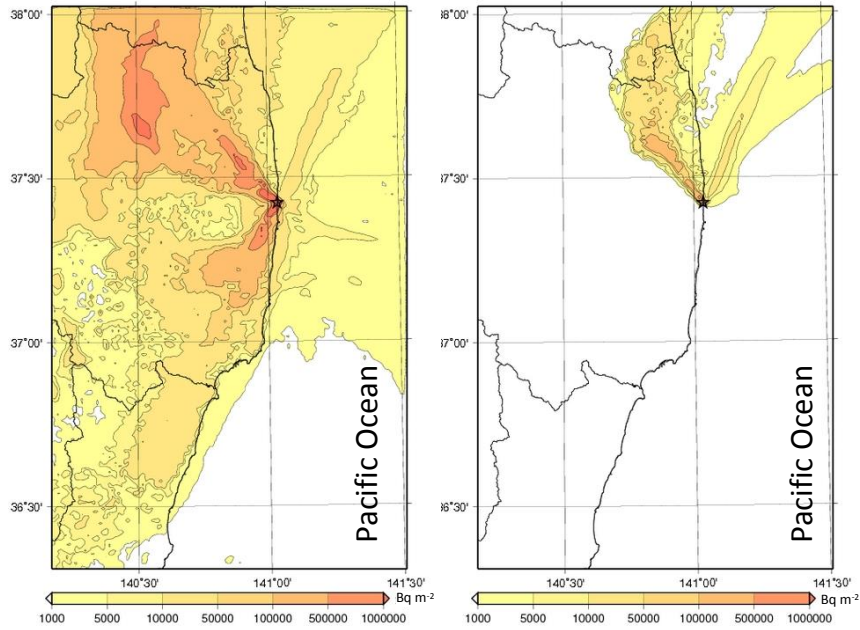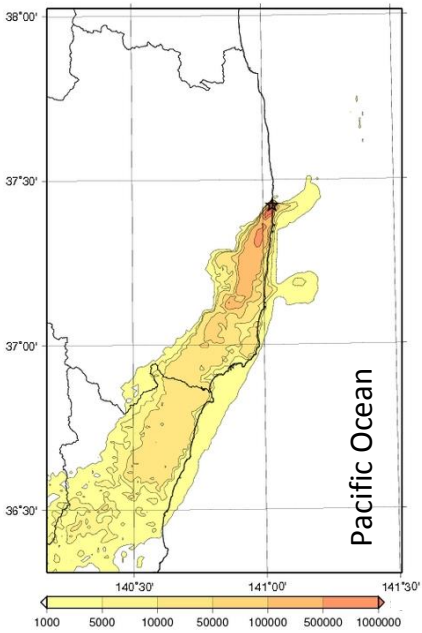
c. 3/14 9 JST－3/15 9 JST   **d**. 3/15 9 JST－3/16 9 JST
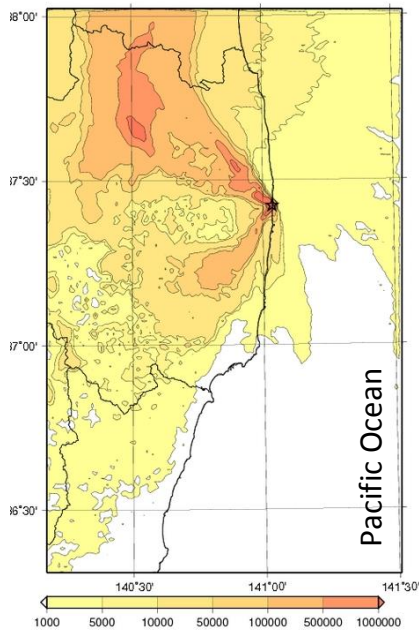
*Color shaded areas: surface deposition of ^{137}Cs (Bq m^{-2})

655

TABLE CAPTIONS

Table 1.

Dust sampling data of ^{131}I at sampling locations in Fig. 1 used for the source term estimation.

Table 2.

Simulation settings for atmospheric dynamic model (MM5) and atmospheric dispersion model (GEARN).

Table 3.

Release duration, release time of radioactive plume, sampling location in Fig. 1, estimated release rate of ^{131}I, meteorological input data for MM5, radioactivity ratios of (^{132}I+^{132}Te)/^{131}I and ^{131}I/^{137}Cs, and estimation method in subsection 2.2 with release height, h.

1 **Table 1**

2

Data code in Fig. 1	Sampling location	Sampling date and time (JST)	^{131}I Concentration (Bq m^{-3})	
			Observed	Calculated[a]
a	Takase[b]	3/12 08:39-3/12 08:49	37	1.0×10^{-12}
b	Kawazoe[b]	3/12 12:00-3/12 12:10	165	1.0×10^{-11}
c	Otabashi[b]	3/13 15:08-3/13 15:18	84	1.0×10^{-12}
d	Tokai (JAEA)[c]	3/15 04:25-3/15 04:45	1260	1.0×10^{-12}

3

4

[a] Calculations were carried out under the assumption of unit release rate (1Bq h^{-1}).
[b] METI (2011a).
[c] JAEA (2011a).

1   **Table 2**

2

	Domain 1	Domain 2	Domain 3
Study areas	Tohoku and Kanto regions in Japan, same as Katata et al. (2011)		
Applied GEARN calculations	No	Yes	Yes
Simulation period for GEARN	5 JST March 12 – 0 JST March 17, 2011		
Horizontal grid cell	100×100	190×130	190×190
Spatial resolutions	9 km	3 km	1 km
Boundary and initial conditions of MM5	Grid Point Value (Global Spectral Model for Japan region, GSM, and Meso-Scale Model, MSM) by Japan Meteorological Agency		
3D/surface analysis nudging[a]	Utilized with wind data at FNPP1 (surface), FNPP2 (120 m), and surface weather stations		
Observation nudging[d]	Utilized with wind data at FNPP1 (surface) and FNPP2 (120 m)		
Release rates and heights	See Table 3		
Other parameters	Same as Katata et al. (2011)		

---

[a] Wind data at FNPP1 and FNPP2 were provided from METI (2011b).

Table 3

No.	Duration (JST)	Release time of sampled air	Data code in Fig. 1	Release rate of ^{131}I (Bq h^{-1})	GPV input data[a]	(^{132}I+^{132}Te)/ ^{131}I[b]	^{131}I/^{137}Cs[f]	Estimation method in subsection 2.2
1	3/12 05:00-3/12 09:30	3/12 08:00	a	3.7×10^{13}	GMS	2.0	10	*Method 1*, *h*=20 m
2	3/12 09:30-3/12 15:30	3/12 11:30	b	1.7×10^{13}	GMS	2.0	10	*Method 1*, *h*=120 m
3	3/12 15:30-3/12 16:00	3/12 15:30	—	3.0×10^{15}	MSM	2.0	10	*Method 2*, Volume[c]
4	3/12 16:00-3/13 23:00	3/13 13:00	c	8.4×10^{13}	GMS	1.3	10	*Method 1*, *h*=120 m
5	3/13 23:00-3/14 11:00	3/14 09:00	—	3.6×10^{13}	—	1.3	10	*Method 3*, *h*=120 m
6	3/14 11:00-3/14 11:30	—	—	3.0×10^{15}	—	1.3	10	Assumed same as No. 3[g]
7	3/14 11:30-3/14 21:30	3/14 21:00	—	2.3×10^{13}	GMS	1.3	10	Chino et al. (2011)
8	3/14 21:30-3/15 00:00	3/14 22:30	d	1.3×10^{15}	GMS	1.0	10	*Method 1*, *h*=120 m
9	3/15 00:00-3/15 07:00	3/15 01:00	d	3.5×10^{14}	GMS	1.0	8.8	Chino et al. (2011)
10	3/15 07:00-3/15 10:00	—	—	3.0×10^{15}	MSM	1.0	10	Katata et al. (2011)
11	3/15 10:00-3/15 13:00	—	—	8.0×10^{13}	MSM	1.0	10	Katata et al. (2011)
12	3/15 13:00-3/15 17:00	—	—	4.0×10^{15}	MSM	1.0	10	Katata et al. (2011)
13	3/15 17:00-3/17 00:00	3/16 04:00	d	2.1×10^{14}	GMS	1.0	70	Chino et al. (2011)

[a] GSM is the Global Spectral Model for Japan region, and MSM the Meso-Scale Model.
[b] Values of radioactive ratios were mainly determined from the available dust sampling data (see subsection 2.3).
[c] Volume sources with the sizes of (x, y, z) = (100, 100, 100 m) and (100, 100, 300 m) were assumed for hydrogen explosions at Unit 1 and 3, respectively.